



NASA-CR-200962

11-02-CR  
48627

---

Research Institute for Advanced Computer Science  
NASA Ames Research Center

# Business Jet Wing Design Using Aerodynamic Shape Optimization

**John Gallman, James Reuther, Neal Pfeiffer, William Forrest and David Bernstorf**

**RIACS Technical Report 96.03 January 1996**

**Presented at the AIAA 34th Aerospace Sciences Meeting and Exhibit, January 1996,**  
*AIAA paper 96-0554*

# **Business Jet Wing Design Using Aerodynamic Shape Optimization**

**John Gallman, James Reuther, Neal Pfeiffer, William Forrest and David Bernstorf**

The Research Institute of Advanced Computer Science is operated by Universities Space Research Association, The American City Building, Suite 212, Columbia, MD 21044, (410) 730-2656

---

Work reported herein was sponsored by NASA under contract NAS 2-13721 between NASA and the Universities Space Research Association (USRA).

# Business Jet Wing Design

## Using Aerodynamic Shape Optimization

John W. Gallman, \*

*NASA Ames Research Center, Moffett Field, California*

James J. Reuther †

*RIACS, Moffett Field, California*

Neal J. Pfeiffer, ‡ William C. Forrest, § David J. Bernstorf ¶

*Raytheon Aircraft Company, Wichita, Kansas*

### Abstract

A new method that relies on computational fluid dynamics (CFD) and numerical optimization is used to design a transonic business jet wing. The first step of this new design method is to develop target pressures for a three-dimensional wing design using a two-dimensional airfoil optimization code (MSES-LINDOP). This airfoil optimization method is fast enough to solve a six-point design problem that is representative of an entire aircraft mission in a few minutes. A full-potential finite element code with a solution adaptive cartesian grid (TRANAIR) is used to analyze the wing-body-nacelle configuration and establish the influence of the fuselage mounted nacelles on the wing pressures. The blockage in the flow caused by these nacelles is approximated in a wing-body Euler CFD code (SYN87) with a large bump on the aft fuselage. The SYN87 code also solves an adjoint set of equations to evaluate the flowfield sensitivities in approximately the same time as that required to solve the Euler equations for one flowfield. These flowfield sensitivities enable three dimensional shape optimization in this study with a quasi-Newton optimization routine. The objective function used to design both the fuselage bump and the wing contours was a sum-of-squares of the difference between computed and target wing pressures. Finally, the surface contours are modified slightly with a computer aided drawing machine to reduce manufacturing com-

plexity. Wind tunnel data from the Boeing Transonic Wind Tunnel is in very good agreement with the pressure distributions developed for the 20° swept wing considered in this study. This data shows that the design goals of natural laminar flow at a Mach number of 0.75 and minimum wave drag at a Mach number of 0.80 have been met and provides a validation of the design method developed in this study.

### Nomenclature

$A_i$	magnitude of sine bump used to perturb airfoil coordinates, used as design variable
$c$	wing section chord
$C_L$	aircraft lift coefficient
$C_P, \widetilde{C}_P$	computed and target wing pressure coefficients
$eps$	estimate of objective function precision
$eta$	accuracy parameter for optimization line search
$\mathcal{F}$	locations of surface boundary points
$I$	objective or cost function
$Mach, M$	free stream Mach number
$N$	number of pressure coefficients calculated for a given wing section
$R$	matrix of residuals of flowfield solution
$tol$	convergence tolerance for objective function
$v$	vector of design variables
$w$	flowfield quantities, velocity, density, etc.
$x/c$	abscissa of normalized wing section coordinate
$\mathcal{X}$	locations of flowfield mesh points
$\Delta y/c$	ordinate of perturbation in normalized wing section coordinate
$\alpha$	angle of attack

Copyright © 1996 by the American Institute of Aeronautics and Astronautics, Inc. No copyright is asserted in the United States under Title 17, U.S. Code. The U.S. Government has a royalty-free license to exercise all rights under the copyright claimed herein for Governmental purposes. All other rights are reserved by the copyright owner.

\*Aerospace Engineer, Member AIAA

†Associate Researcher, Member AIAA

‡Senior Technical Specialist, Member AIAA

§Engineer, Applied Aerodynamics, Member AIAA

¶Project Engineer, Member AIAA

$\psi$

vector of Lagrange Multipliers

## Subscripts

i, j	counters for spanwise and chordwise location of pressure coefficients
w	wing

## Introduction

Recently, a healthy business jet industry has pursued the development of faster aircraft with significant increases in range.<sup>1, 2, 3</sup> Unlike previous business jets developed for cruising speeds near a Mach number of 0.70, these new aircraft with cruise speeds near  $M = 0.8$  require wings with more sweep and carefully designed airfoil sections that minimize the onset of compressibility drag. Furthermore, these high speed wings must be compatible with typical business jet configurations that have engines mounted on the fuselage near the wing trailing edge. These requirements create an aerodynamic design problem that benefits from modern computational fluid dynamics (CFD) and aerodynamic shape optimization.

Several recent developments in aerodynamic sensitivity analysis and the application of CFD to business jet design problems make it possible to develop a modern transonic wing in a few months. Chandrasekharan, et. al.<sup>4</sup> showed that TRANAIR,<sup>5, 6</sup> a full-potential, CFD code with an adaptive cartesian grid, could be used to reduce the cruise drag of an existing aircraft by tailoring the geometry near the wing root and in the nacelle pylon area. Gallman, et. al.<sup>7</sup> used a combination of wing-alone optimization with R22OPT<sup>8, 9, 10</sup> and entire configuration analyses with TRANAIR to design a transonic business jet wing for a cruise Mach number of 0.83. Recent Developments in aerodynamic sensitivity analysis<sup>11, 12, 13</sup> promise significant improvement in the design process. Reference 11 presents the development of a set of adjoint equations that enable inexpensive calculation of flowfield sensitivities. This approach is particularly appealing because it produces the gradient of an aerodynamic objective function with respect to the design variables within the same computational time and memory as a single flowfield analysis. This is in contrast to a finite difference approximation of the gradient that requires  $n + 1$  flowfield analyses, where  $n$  is the number of design variables.

This paper presents the application of the SYN87 design code of Ref. 11 and TRANAIR to the design of a Mach = 0.80 business jet wing with 20° of wing sweep. Figure 1 shows the baseline configuration considered in this study. Since SYN87 was limited to wing-body configurations, a design process was developed that includes the approximation of a

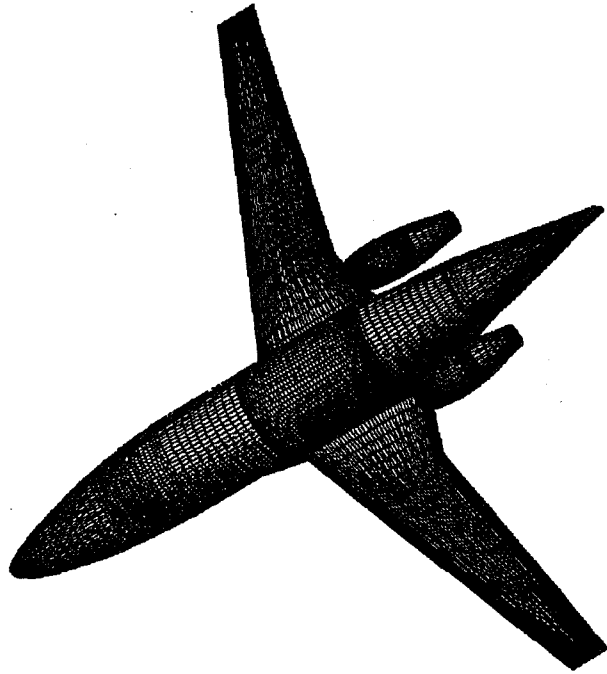


Fig. 1 Baseline wing-body-nacelle configuration.

nacelle-pylon configuration with a large bump on the aft fuselage. This "bump" approximation was first used by Hicks in Ref. 17 to simulate the influence of fuselage mounted engines on the wing pressures and to avoid the complexity of a multi-block flowfield grid. Figure 2 shows an isometric view of a SYN87 wing-body-bump model. Full configuration analyses with TRANAIR are used to validate the bump approximation and to design the wing-body fillet. A description of the new design process is followed by a discussion of the design results, and a comparison with wind tunnel data.

## Analysis and Optimization Methods

The CFD codes used in this study are compatible with a fast turn around design process because they require simple input files and automate the flowfield grid generation. SYN87, used here for wing optimization, is based on Jameson's FLO87<sup>14, 15</sup> code, which solves the Euler equations using a cell-centered finite volume scheme with residual averaging and multigrid acceleration. The SYN87 code also includes a wing-body grid generator and an efficient calculation of the aerodynamic-sensitivity derivatives. TRANAIR is a full-potential, finite-element code with a solution-adaptive, cartesian grid. This CFD code requires surface-panel geometry as input. TRANAIR was used to assess the interference of the nacelle and pylon on the wing pressures and to design the surface shape of the wing-body fillet. Drela's MSES and LINDOP<sup>16</sup> airfoil design package provided target pressure

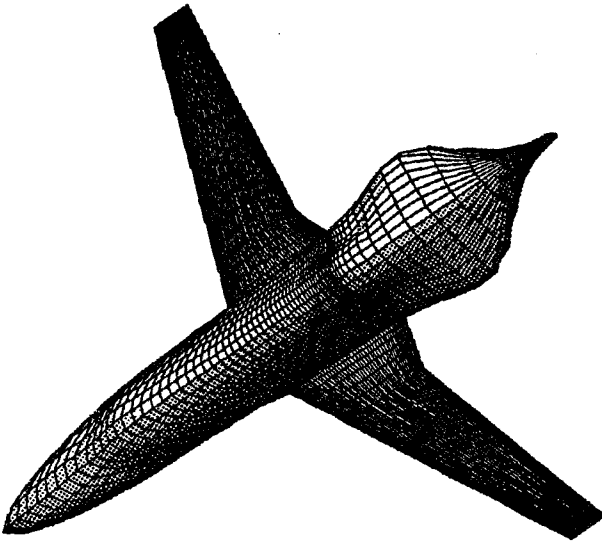


Fig. 2 Bump approximation of nacelle pylon configuration.

distributions for the three dimensional wing.

### Multipoint Airfoil Optimization

The interactive airfoil design and optimization framework of MSES/LINDOP enabled the solution of an aerodynamic design problem based on six flight conditions. This code solves a coupled Euler/Boundary-layer flowfield with a full Newton solution method that provides the value of the aerodynamic objective function and the flowfield sensitivities or gradients required for optimization. The full Newton solution method provides the gradients with respect to pre-defined airfoil design variables for a fraction of the cost of one flowfield solution,<sup>16</sup> thereby accomplishing the equivalent of the adjoint solution technique used by SYN87.

Airfoil optimization studies based on objective functions defined by a sum of  $C_d$  or  $ML/D$  for six flight conditions identified the compromise between the potential for laminar flow at  $M = 0.75$  and the requirement for minimum wave drag at  $M = 0.80$ . The angle of attack and 20 Chebyshev polynomial perturbations to the airfoil coordinates represented the design variables that created optimum airfoils with a constraint on maximum thickness. Evaluation of the pressure distributions and drag characteristics every 6-8 optimization steps frequently led to a slight modification or redefinition of the design problem (objective function). Solutions to airfoil optimization problems that focused on reducing wave

drag at  $M = 0.80$ , on the development of favorable pressure gradients for laminar flow at  $M = 0.75$ , or on a weighted combination of these design goals helped identify the key trade-offs. A compromise between these two aerodynamic goals was then used to define the target pressure distributions used in the wing design process described in the next paragraph. Once the three dimensional design process was underway, the design-to-target-pressure option in LINDOP was used to duplicate the wing pressures in two dimensions. This enabled efficient evaluation of the current wing at six design points and guided the development of target pressures for 3D wing optimization.

### Wing Design Process

Figure 3 shows a flow chart of the process used to design a transonic business jet wing for low wave drag at  $Mach = 0.80$  and for natural laminar flow for all Mach numbers between 0.75 and 0.80. The MSES/LINDOP design tool is used to develop some preliminary airfoils and to gain a thorough understanding of the six-point design problem. A TRANAIR analysis is then used to establish the influence of the nacelles on the wing and to evaluate the wing pressures. This analysis provides the wing pressure targets for the SYN87 optimization of a bump on the aft fuselage. The wing design problem is now defined with target pressures at  $Mach = 0.80$ . Airfoil optimization enables the definition of these targets such that the resulting wing will have low wave drag at  $M = 0.80$  and the potential for natural laminar flow at  $M = 0.75$ . Typically, these targets are also perturbations of the wing pressures obtained in a previous wing optimization. This creates a series of design objectives that are small perturbations from an existing wing and ensures that the targets represent an achievable goal. Finally, SYN87 is used with a fixed fuselage bump to design a wing that minimizes a sum-of-squares measure of the difference between the computed and target pressure distributions. At this point it usually becomes necessary to reloft the new wing, and to modify the fairing that blends the wing into the body. This lofting step, achieved with a computer aided drawing machine, reduces manufacturing complexity, ensures that the landing gear fit in the wing, and accurately quantifies the wing fuel volume. As shown in Fig. 3, the process now returns to an analysis of the wing-body-nacelle configuration to evaluate the current design.

### Optimization

The fuselage bump and wing design problems were solved using the unconstrained quasi-Newton optimization routine of QNMDIF.<sup>18, 19</sup> The objective function for both problems is the sum-of-squares of

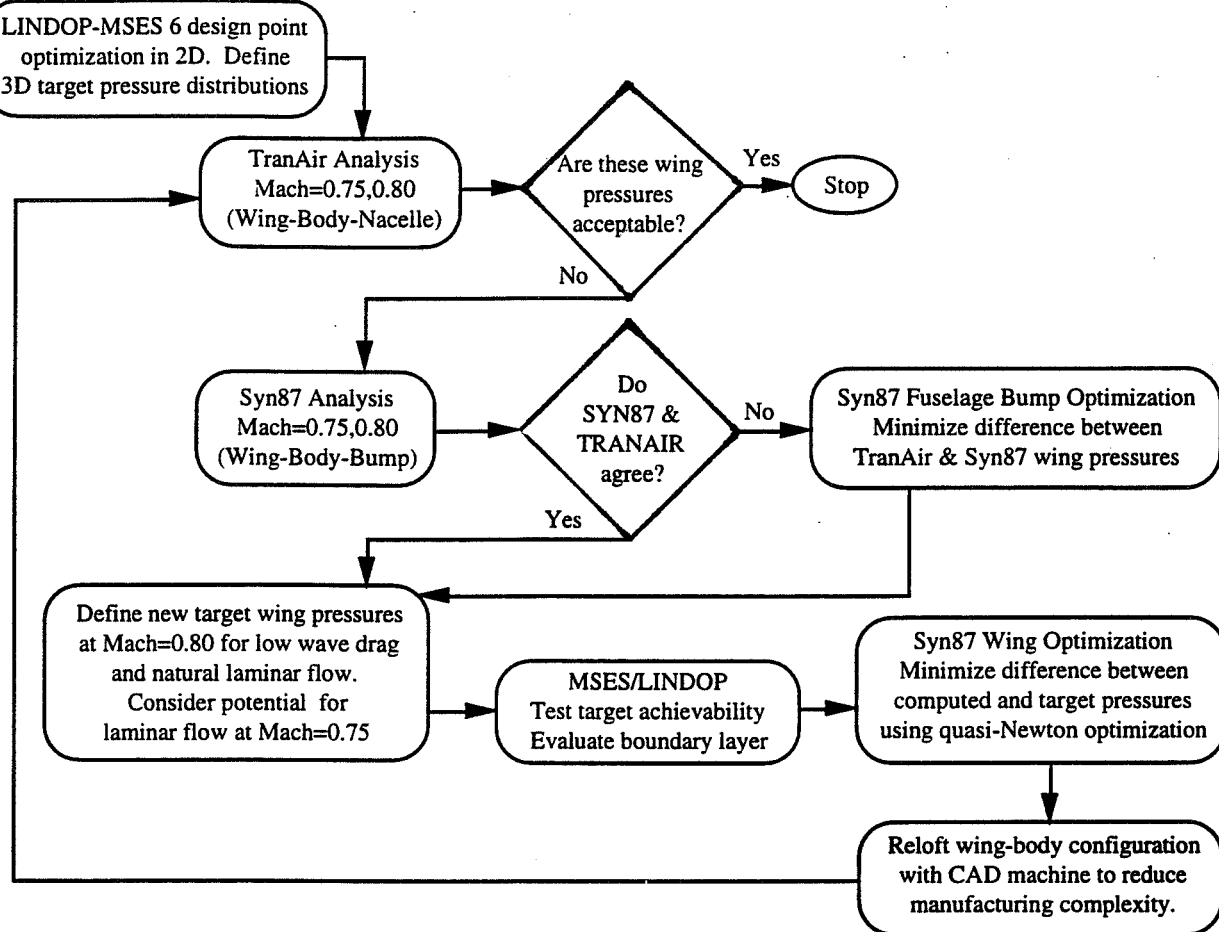


Fig. 3 Flowchart of design process.

the difference between computed and target wing pressures given by

$$I = 0.2 \sum_{i=1}^7 \sum_{j=1}^{N_j} \left( C_{P_{i,j}} - \bar{C}_{P_{i,j}} \right)^2 \quad (1)$$

where  $i$  indicates a specific wing section,  $j$  represents the chordwise location of the computed and target pressure coefficients, and  $N_j$  is the number of target points at station  $j$ . Target wing pressures were defined at 14%, 21%, 30%, 47%, 66%, 82%, and 100% semispan. The wing surface was constructed by lofting linearly between streamwise airfoil sections at 14%, 21%, 30%, 65%, and 100% semispan. Twenty five design variables define the magnitudes of sine wave perturbations to the airfoil upper or lower surface at each of the wing defining stations. These perturbations to the airfoil coordinates are given by

$$\Delta y/c = \sum_{i=1}^{25} A_i \sin^2 \left[ \pi (x/c)^{\ln(0.5)/\ln(i/26)} \right] \quad (2)$$

This type of sine wave was also used to perturb the aft-fuselage for the "bump" approximation of the

nacelle-pylon configuration. Although explicit constraints on wing thickness were not included in the objective function (Eq. 1), a wing fuel volume constraint influenced the definition of target pressures throughout this design study. Each optimization iteration of either a wing or bump design problem involves the calculation of a desirable search direction using the gradient of the objective function and an accumulated approximation of second derivatives, followed by a line search through the design space, and a test for convergence. Input values for the precision of the objective function ( $\text{eps}$ ), an accuracy or convergence parameter for each line search ( $0 \leq \text{eta} \leq 1$ ), and an optimality tolerance ( $\text{tol} = 0.1$ ) for the gradient of the objective function control the computational tests for convergence in QNMDIF. A fairly accurate line search ( $\text{eta} = 0.2$ ) reduced the number of line searches required for convergence and improved the accumulated approximation of the second derivatives. The convergence of the iterative flow solver provided an estimate of function precision ( $\text{eps} = 10^{-3}$ ). For the optimization problem considered in this study, reductions in the objective function gradient below

$10^{-1}$  produce imperceptible design improvements or variations in the objective function that are less than the input function precision. The design process presented in Fig. 3 does not require convergence to the Khun-Tucker conditions for optimality and encourages an assessment of the design improvement after every few line searches or design iterations.

### Adjoint Equation Gradients

SYN87 was used to solve the Euler equations and their related adjoint equations on a 193x49x41 mesh using the explicit methods of Refs. 14, 15. The adjoint equations enable the solution of the objective function gradient for an unlimited number of design variables.<sup>11</sup> To see how these adjoint equations enable the efficient calculation of gradient information, consider an objective function given by

$$I = I(w, \mathcal{X}, \mathcal{F}), \quad (3)$$

and a set of flowfield equations represented by

$$R(w, \mathcal{X}, \mathcal{F}) = 0, \quad (4)$$

where  $w$  represents the flowfield quantities,  $\mathcal{X}$  represents the physical locations of the mesh points within the computational domain, and  $\mathcal{F}$  represents the physical location of the boundary. The adjoint equation is formulated by combining the gradient in the objective function

$$\begin{aligned} \left\{ \frac{\partial I}{\partial v} \right\}^T &= \left\{ \frac{\partial I}{\partial w} \right\}^T \left[ \frac{\partial w}{\partial v} \right] \\ &+ \left\{ \frac{\partial I}{\partial \mathcal{X}} \right\}^T \left[ \frac{\partial \mathcal{X}}{\partial v} \right] + \left\{ \frac{\partial I}{\partial \mathcal{F}} \right\}^T \left[ \frac{\partial \mathcal{F}}{\partial v} \right] \end{aligned} \quad (5)$$

and the gradient in the flowfield equations

$$\begin{aligned} \left[ \frac{\partial R}{\partial v} \right] &= \left[ \frac{\partial R}{\partial w} \right] \left[ \frac{\partial w}{\partial v} \right] \\ &+ \left[ \frac{\partial R}{\partial \mathcal{X}} \right] \left[ \frac{\partial \mathcal{X}}{\partial v} \right] + \left[ \frac{\partial R}{\partial \mathcal{F}} \right] \left[ \frac{\partial \mathcal{F}}{\partial v} \right] = 0 \end{aligned} \quad (6)$$

After introducing  $\psi$ , a vector of Lagrange Multipliers, Eqs. 5 and 6 are summed

$$\left\{ \frac{\partial I}{\partial v} \right\}^T = \left\{ \frac{\partial I}{\partial w} \right\}^T - \left\{ \psi \right\}^T \left[ \frac{\partial R}{\partial v} \right]$$

or

$$\begin{aligned} \left\{ \frac{\partial I}{\partial v} \right\}^T &= \left\{ \left\{ \frac{\partial I}{\partial w} \right\}^T - \left\{ \psi \right\}^T \left[ \frac{\partial R}{\partial w} \right] \right\} \left\{ \frac{\partial w}{\partial v} \right\} \\ &+ \left\{ \left\{ \frac{\partial I}{\partial \mathcal{X}} \right\}^T - \left\{ \psi \right\}^T \left[ \frac{\partial R}{\partial \mathcal{X}} \right] \right\} \left\{ \frac{\partial \mathcal{X}}{\partial v} \right\} \\ &+ \left\{ \left\{ \frac{\partial I}{\partial \mathcal{F}} \right\}^T - \left\{ \psi \right\}^T \left[ \frac{\partial R}{\partial \mathcal{F}} \right] \right\} \left\{ \frac{\partial \mathcal{F}}{\partial v} \right\} \end{aligned} \quad (7)$$

Since  $\psi$  in Eq. 7 is arbitrary, it may be chosen such that

$$\left[ \frac{\partial R}{\partial w} \right]^T \left\{ \psi \right\} = \left\{ \frac{\partial I}{\partial w} \right\} \quad (8)$$

is satisfied. The gradient in the objective function then becomes

$$\begin{aligned} \left\{ \frac{\partial I}{\partial v} \right\}^T &= \left\{ \left\{ \frac{\partial I}{\partial \mathcal{X}} \right\}^T - \left\{ \psi \right\}^T \left[ \frac{\partial R}{\partial \mathcal{X}} \right] \right\} \left\{ \frac{\partial \mathcal{X}}{\partial v} \right\} \\ &+ \left\{ \left\{ \frac{\partial I}{\partial \mathcal{F}} \right\}^T - \left\{ \psi \right\}^T \left[ \frac{\partial R}{\partial \mathcal{F}} \right] \right\} \left\{ \frac{\partial \mathcal{F}}{\partial v} \right\} \end{aligned} \quad (9)$$

where  $\left[ \frac{\partial R}{\partial \mathcal{F}} \right]$  and  $\left\{ \frac{\partial I}{\partial \mathcal{X}} \right\}^T$  are zero since the surface boundary points are considered separately from the surface mesh points and the objective function is defined in terms of flowfield quantities that are evaluated on the surface boundary. All terms except for  $\psi$  are calculated inexpensively using finite differences since they only depend on the boundary surface  $\mathcal{F}$  and the mesh  $\mathcal{X}$ . The computational time required to solve Eq. 8 is approximately equal to the time required to solve the Euler equations for one flowfield. Since a very small amount of computational time is then required to solve Eq. 9 for each design variable, the total time required for a gradient calculation is insensitive to the number of design variables.

### Example SYN87 Wing Optimization

Approximately 10 loops through the design process presented in Fig. 3 produced an acceptable wing design in this study. However, only two bump optimizations were required to approximate the influence of the nacelles on the wing. It is difficult to select a wing optimization case from this study that accurately demonstrates the power of SYN87 because these wing optimization cases were used to test the development of improved boundary conditions for the solution of the adjoint equations.

An example wing design problem was constructed to demonstrate the performance of the SYN87 design tool by replacing the defining sections of the final wing at 30%, 65%, and 100% semispan with NACA-0012 sections that have been scaled to the thickness of the final wing. The wing sections at 14%, and 21% remain unchanged. The design objective was to recover the final wing design by specifying the pressure distribution for this wing over the entire span. Fifty design variables (Eq. 2) placed at 30%, 65%, and 100% semispan define the wing optimization problem. Figure 4 shows the initial and target pressure at 48% semispan. This span station is halfway between the defining stations at 30% and 65% semispan and the last to converge. Figures 5-8 show the level of convergence to the target pressures after 3, 5, 7, and 26 optimization iterations. After 3 line searches or optimization iterations, the shock location and strength match the target, but the pressure recovery section is still quite different from the target (see Fig. 5). Figure 6 shows good agreement between the design and target pressures after just five optimization steps. Seven optimization steps, shown in Fig. 7, take approximately

6 hours on a Cray C90 and represent the level of convergence typical for the design process shown in Fig 9. Figure 8 shows that 26 optimization iterations and 16 hours on a Cray C90 produce a nearly perfect match between the pressures and recovers the final wing section coordinates precisely.

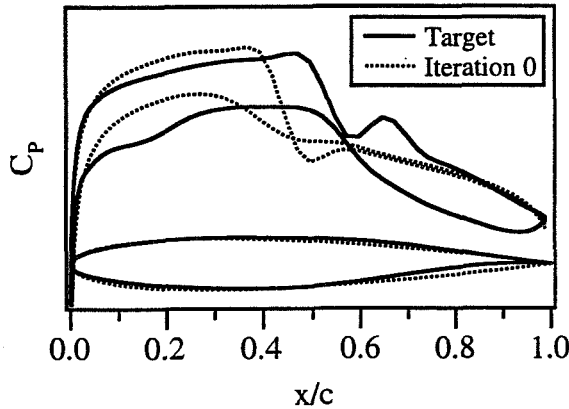


Fig. 4 Analysis of example wing and target pressures.

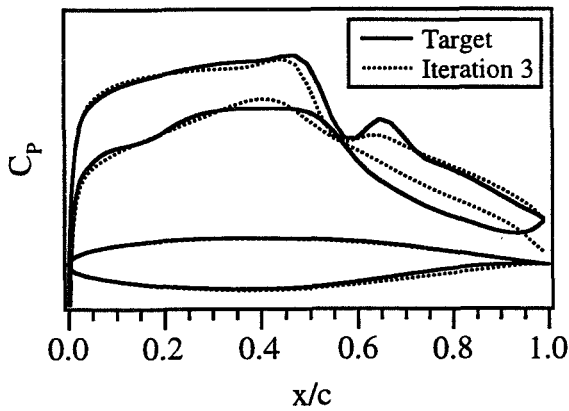


Fig. 5 Convergence in  $C_P$  after 3 optimization steps.

## Results

The MSES-LINDOP airfoil design code enabled the development of target pressures that include the compromise necessary for acceptable performance at all of the flight conditions listed in Table 1. The design goals established for these flight conditions include

- Natural laminar flow in both upper and lower surface wing boundary layers for cruise Mach numbers greater than 0.75.
- A minimum amount of nose down pitching moment

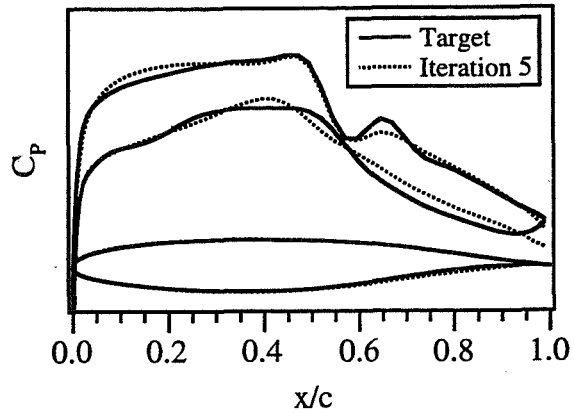


Fig. 6 Convergence in  $C_P$  after 5 optimization steps.

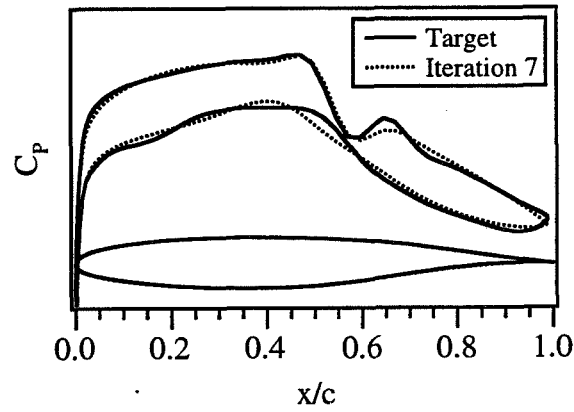


Fig. 7 Convergence in  $C_P$  after 7 optimization steps.

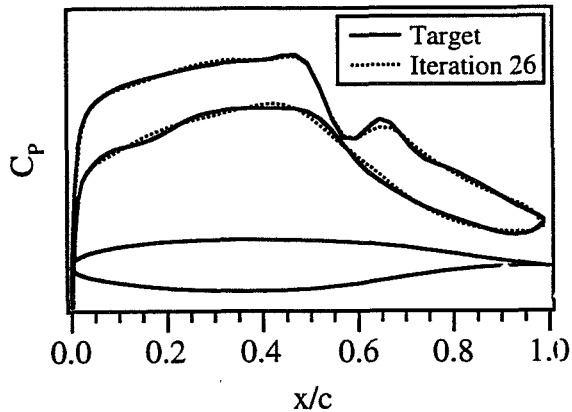


Fig. 8 Typical convergence in  $C_P$  after 26 optimization steps.

- A limit on the aft loading of wing section pressure distributions to enable manual aileron controls.
- Wave drag characteristics that lead to efficient high speed cruise with an overspeed margin of 0.03 in Mach number.
- Wing fuel volume sufficient to meet mission range requirements.
- Wing surface contours that facilitate simple low cost manufacturing.

Fortunately, specific constraints were not necessary to limit the aft loading and reduce the nose down pitching moment. Unlike other inviscid airfoil optimization studies that lead to significant aft loading in an attempt to reduce the wave drag, the viscous portion of the objective function considered by LINDOP created more favorable pressure gradients and an acceptable amount of aft loading. The quarter chord wing sweep of the baseline configuration was limited to 20° in an attempt to limit the crossflow in the boundary layer and increase the potential for natural laminar flow. Unfortunately, finite wing effects, flow acceleration caused by the fuselage, and the effective blockage created by the fuselage mounted nacelles were sufficient to produce unacceptable wing pressures after the initial two dimensional airfoils were used to construct a wing using simple-sweep theory. Figure 9 shows pressure distributions at the chord break for this initial wing both with and without the influence of the nacelles. Note the unacceptable shocks on both the upper and lower surface and the significant influence of the nacelle model on the wing pressures. Although the results of Fig. 9 suggest that airfoil optimization is of limited value in determining the final wing design, MSEs/LINDOP was invaluable when it came to understanding the trade-off between the potential for laminar flow and minimum wave drag. The traditional flat-top supercritical pressure distribution with a significant amount of aft loading led to leading edge pressure peaks and adverse pressure distributions with limited potential for natural laminar flow at Mach numbers below the design point. Throughout the wing design process presented in Fig. 3, multi-point airfoil optimization guided the selection of target pressures. For example, duplicating the 3D wing pressures in 2D made it possible to evaluate the influence of a modification to the wing pressures at  $M=0.80$  on the other five flight conditions.

The extreme difference in the wing-body and wing-body-nacelle pressures shown in Fig. 9 emphasizes the need to include the nacelles in the aerodynamic analysis. Nacelle inlet and outlet boundary conditions that approximate the cruise flight condition and nacelle interference with the fuselage create a large blockage in

Mach	Flight Condition
0.80	High Speed Cruise
0.75	Medium Speed Cruise
0.70	Low Speed Cruise
0.83	1g Overspeed
0.80	1.3g Maneuver
0.70	Climb

Table 1 Flight conditions for multi-point wing optimization.

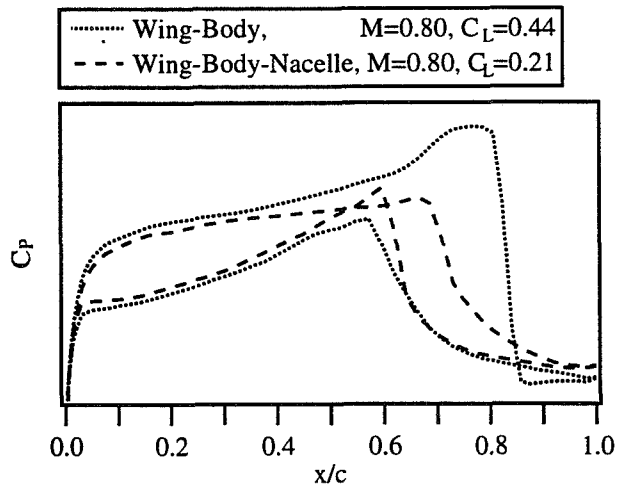


Fig. 9 Representative pressure distributions for the initial wing at a fixed angle of attack.

the flow. This blockage reduces the wing lift, even near the tip, at a fixed angle of attack and Mach number. Figures 10–15 show the influence of the nacelle blockage on the final wing design. Figures 10 and 11 show that the nacelle blockage moves the shock forward approximate 20% chord for the inboard portion of the wing and Fig. 12 shows a forward shift of 15% in shock location at 65% semispan. These figures also show excellent agreement between the pressures calculated using the wing-body-bump model of SYN87 and the wing-body-nacelle model of TRANAIR at approximately the same lift coefficient. The bump approximation was found to be quite robust with respect to changes in the free stream Mach number and to changes in the incidence of the wing with respect to the body, created during the relofting step shown in Fig. 3. Figures 13–15 demonstrate the accuracy with which the fuselage bump can approximate the nacelles at a Mach number of 0.75, even though it was designed to simulate the blockage caused by the nacelles at Mach=0.80. Figures 10–15 also demonstrate the insensitivity of the bump approximation to the relofting step of the design process, since the TRANAIR model has 0.5° more wing incidence relative to the fuselage than the SYN87 model.

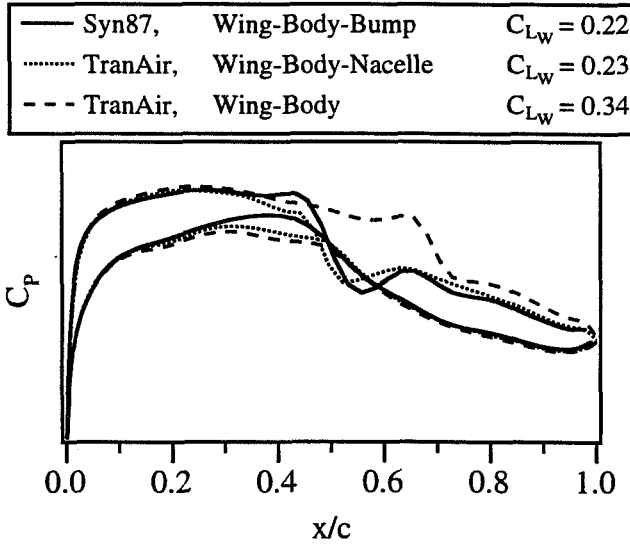


Fig. 10 Wing pressure distributions at 21% semispan for optimized wing at Mach=0.80.

The design objectives of low wave drag and natural laminar flow are satisfied with the pressures shown in Figures 10–15. At Mach=0.80, Figs. 10–12 show favorable pressure distributions to about 45% chord on the upper surface and almost 50% chord on the lower surface indicating the potential for natural laminar flow. Local Mach numbers less than 1.3 on the wing upper surface produce weak shock waves at approximately 50% chord along the entire span of the

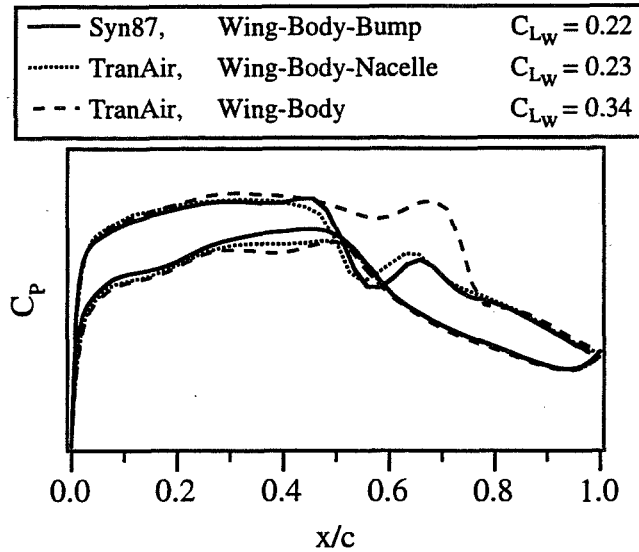


Fig. 11 Wing pressure distributions at 30% semispan for optimized wing at Mach=0.80.

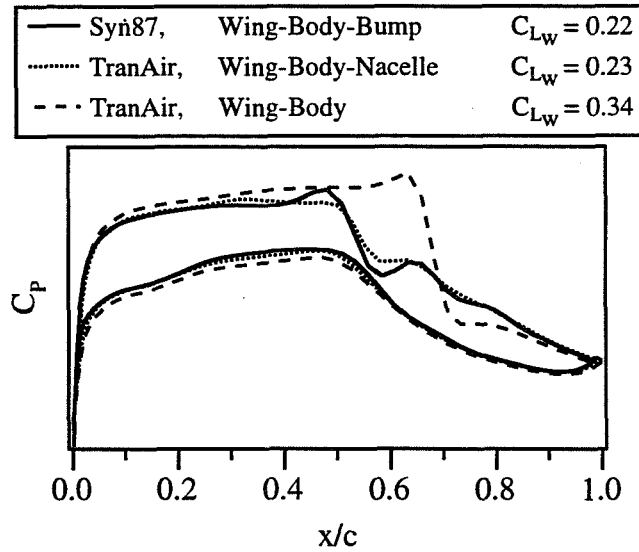


Fig. 12 Wing pressure distributions at 65% semispan for optimized wing at Mach=0.80.

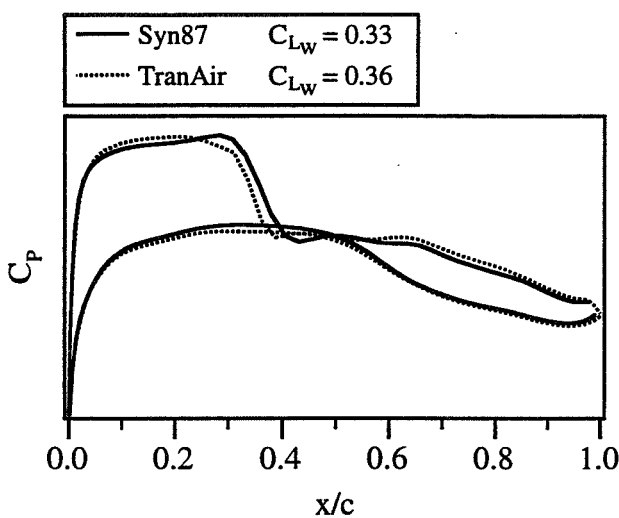


Fig. 13 Wing pressure distributions at 21% semispan for optimized wing at Mach=0.75.

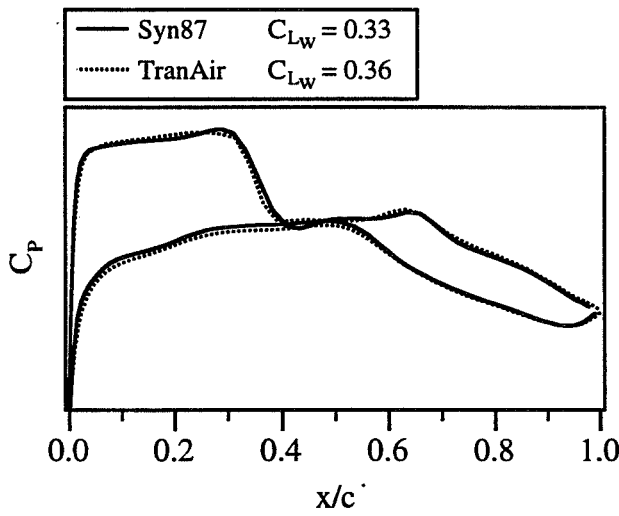


Fig. 14 Wing pressure distributions at 30% semispan for optimized wing at Mach=0.75.

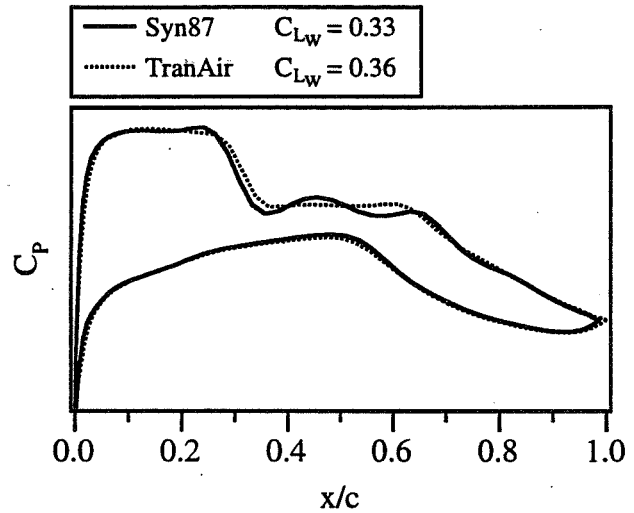


Fig. 15 Wing pressure distributions at 65% semispan for optimized wing at Mach=0.75.

wing. This produces a constant shock sweep angle of  $16.5^\circ$ , even inboard of the chord break where the trailing edge is swept forward. These figures also show a slight reacceleration after the shock which could lead to boundary layer separation problems, but which will also keep the shock from growing as it moves aft with increases in free stream Mach number. Figures 13-15 show the potential for natural laminar flow to approximately 30% chord on the upper surface and 50% chord on the lower surface at a cruise Mach number of 0.75. Once again the weak shock is located at a constant chordwise location, 35%, along the entire semispan.

A 1/8 scale model was tested in the Boeing Transonic Wind Tunnel to validate our design process. Although the wing contours remain the same, the aft fuselage of this model is different from the fuselage used in the wing design process and in the analysis presented in Figs. 10-15. The improved aft fuselage reduced the shock strength between the fuselage and the nacelle which creates a slight reduction in the influence on the wing pressures. The test results presented in Figs. 16 and 17 for a Mach number of 0.80 were measured at an angle of attack of  $0.88^\circ$ , and a Reynolds number of  $2.5 \times 10^6$ . Figures 18 and 19 show the pressures measures for a Mach number of 0.75 at angle of attack of  $1.4^\circ$ , and a Reynolds number of  $2.4 \times 10^6$ . For most of the test, transition disks were placed one inch aft of the wing leading edge (approx. 15% chord), around the aircraft nose, and near the leading edge of all other aircraft components. Without transition disks on the wing leading edge, flow visualization based on infrared thermography showed that a laminar boundary layer persisted to the onset

of the shock wave. These results provide an assessment of the accuracy of the TRANAIR analyses and a validation of the inviscid design methods used in this study.

Figures 16-19 show a comparison of experimental data and TRANAIR analyses performed both with and without a strip boundary layer on the wing. The excellent agreement between the analysis with a boundary layer and the experimental data indicates that the effects of aeroelastic deflection of the solid steel model or interference from the slotted wind tunnel walls are negligible. As expected, the boundary layer moves the shock location forward and reduces the lift coefficient at the same angle of attack. These figures also show that the full-potential shocks in the TRANAIR solutions agree with the experiment data and indicate that the design goals of weak shock waves and low wave drag have been achieved. Figures 16-17 also show favorable pressure distributions with the potential for natural laminar flow, even at a slightly higher angle of attack and lift coefficient than the design condition presented in Figs. 10-12. At Mach=0.75, Figs. 18 and 19 show a slight reduction in the potential for upper surface laminar flow and a constant chordwise location of a weak shock wave. These results validate the wing optimization methods based on SYN87 and the TRANAIR calculations.

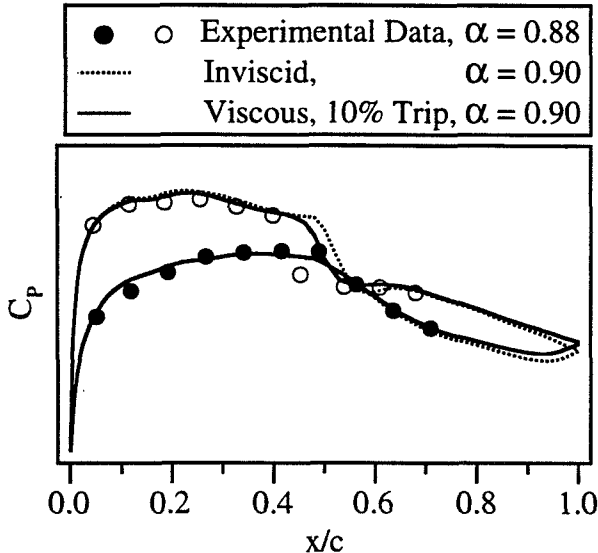


Fig. 16 TRANAIR and wind tunnel pressures at 21% semispan for optimized wing at Mach=0.80.

## Conclusions

A transonic wing of a high speed business jet was designed using a new iterative design process that includes wing-body optimization and wing-body-nacelle

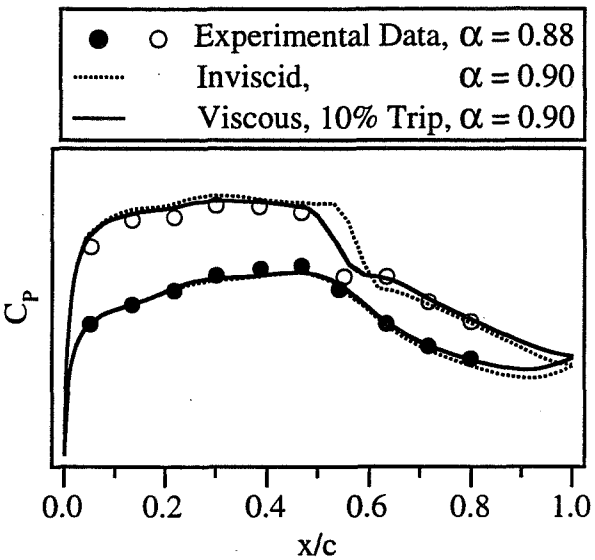


Fig. 17 TRANAIR and wind tunnel pressures at 52% semispan for optimized wing at Mach=0.80.

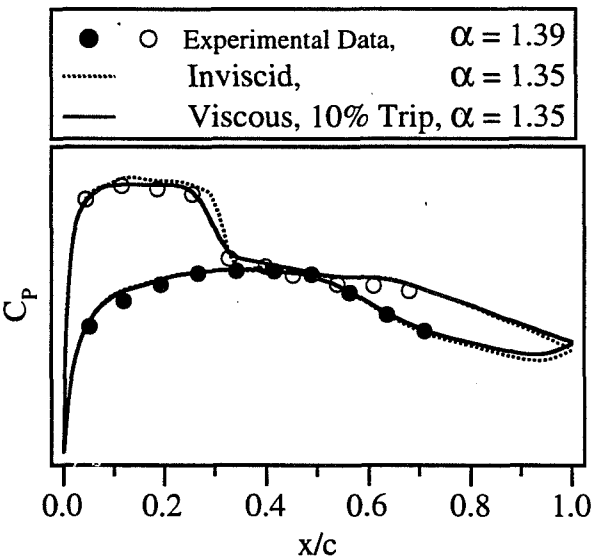


Fig. 18 TRANAIR and wind tunnel pressures at 21% semispan for optimized wing at Mach=0.75.

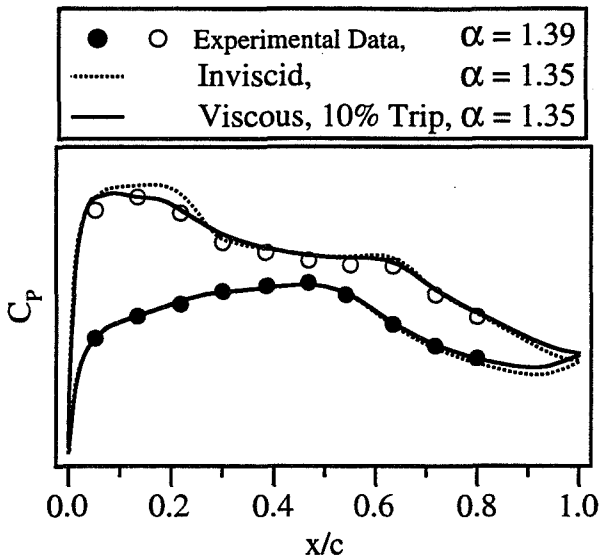


Fig. 19 TRANAIR and wind tunnel pressures at 52% semispan for optimized wing at Mach=0.75.

analysis. Full-potential analysis of the wing-body-nacelle configuration provided an accurate assessment of the influence of the fuselage mounted engines on the wing pressures. This aerodynamic interference was approximated with the wing-body optimization code by designing a bump on the aft fuselage. This bump was quite effective at capturing the influence of the nacelles on the wing pressure distributions and enabled the application of the wing-body code to the wing-body-nacelle design problem. The wing-body optimization tool, SYN87, solves the Euler equations using a cell-centered finite volume scheme with residual averaging and multigrid acceleration. This design tool also includes an automatic wing-body grid generator and an adjoint-equation solver that produces the gradient of the objective function in approximately the same computational time as the solution of the flowfield equations. This approach to the optimization problem led to computational times of approximately 6 hours on a Cray C-90 for 7 optimization steps or line searches through a design space defined by 150 variables. The final wing designed in this study satisfies the requirements for low wave drag at Mach = 0.80 and the potential for natural laminar flow at Mach numbers between 0.75 and 0.80. Pressure distributions measured in the Boeing Transonic Wind Tunnel are in excellent agreement with calculations for the final wing design. These results provide some validation of the SYN87 wing optimization tool and indicate that three dimensional aerodynamic shape optimization is now practical for a fast paced aircraft development project.

## References

<sup>1</sup>Dornheim, M. A., "Dassault's Falcon 2000: New Big Cabin Twinjet," *Aviation Week & Space Technology*, pp. 42-45, March 29 1993.

<sup>2</sup>McKenna, J. T. and North, D. M., "Corporate Operators Pursue High-Value Products at NBAA," *Aviation Week & Space Technology*, pp. 27-28, Sept. 27 1993.

<sup>3</sup>North, D. M., "IAI Launches Galaxy into Crowded Market," *Aviation Week & Space Technology*, p. 29, Sept. 27 1993.

<sup>4</sup>Chandrasekharan, R. M., Hawke, V. M., Hinson, M. L., Kennelly, Jr., R. A., and Madson, M. D., "Aerodynamic Tailoring of the Learjet Model 60 Wing," Presented at SAE Aerotech, Costa Mesa, California, SAE Paper 932534, Sept. 27-30 1993.

<sup>5</sup>Johnson, F. T., Samant, S. S., Bieterman, M. B., Melvin, R. G., Young, D. P., Bussoletti, J. E., and Hilmes, C. L., "TranAir: A Full-Potential Solution-Adaptive Rectangular Grid Code for Predicting Subsonic, Transonic, and Supersonic Flows About Arbitrary Configurations, Theory Document," Contractor Report 4348, NASA, Dec. 1992.

<sup>6</sup>Johnson, F. T., Samant, S. S., Bieterman, M. B., Melvin, R. G., Young, D. P., Bussoletti, J. E., and Hilmes, C. L., "TranAir: A Full-Potential Solution-Adaptive Rectangular Grid Code for Predicting Subsonic, Transonic, and Supersonic Flows About Arbitrary Configurations, User Guide," Contractor Report 4349, NASA, Dec. 1992.

<sup>7</sup>Gallman, J. W., Madson, M. D., Kennelly, Jr., R. A., Chandrasekharan, R. M., Hawke, V. M., and Hinson, M. L., "Optimization of a Transonic Business Jet Wing," Presented at Presented at AIAA Aerospace Sciences Meeting and Exhibit, Reno, NV, AIAA Paper 95-0041, Jan. 9-12 1995.

<sup>8</sup>Jameson, A. and Caughey, D. A., "Numerical Calculation of the Transonic Flow Past a Swept Wing," Contractor Report 153297, NASA, June 1977.

<sup>9</sup>Arieli, R., Tauber, M. E., Saunders, D. A., and Caughey, D. A., "Computation of Transonic Flow about Helicopter Rotor Blades," *AIAA Journal*, Vol. 24, May 1986.

<sup>10</sup>Tauber, M. E. and Langhi, R. G., "Transonic Rotor Tip Design Using Numerical Optimization," Technical Memorandum 86771, NASA, Oct. 1985.

<sup>11</sup>Reuther, J. and Jameson, A., "Aerodynamic Shape Optimization of Wing and Wing-Body Configurations Using Control Theory," Presented at Presented at AIAA Aerospace Sciences Meeting and Exhibit, Reno, NV, AIAA Paper 95-0123, Jan. 9-12 1995.

<sup>12</sup>Burgreen, G. W. and Baysal, O., "Three Dimensional Aerodynamic Shape Optimization of Wings Using Sensitivity Analysis," Presented at Presented at AIAA Aerospace Sciences Meeting and Exhibit, Reno, NV, AIAA Paper 94-0094, Jan. 1994.

<sup>13</sup>Korivi, V. M., Taylor III, A. C., and Newman, P. A., "Aerodynamic Optimization Studies Using a 3-D Supersonic Euler Code with Efficient Calculation of Sensitivity Derivatives," in *Fifth AIAA/USAF/NASA/ISSMO Symposium on Multi-disciplinary Analysis and Optimization*, Panama City Beach, FL, AIAA Paper 94-4270, Sept. 7-9, 1994.

<sup>14</sup>Jameson, A., "Solution of the Euler Equations by a Multigrid Method," *Applied Mathematics and Computations*, Vol. 13, pp. 327-356, 1983.

<sup>15</sup>Jameson, A., "Multigrid Algorithms for Compressible Flow Calculations," in *Proceedings of the 2nd European Conference on Multigrid Methods, Cologne, 1985, Lecture Notes in Mathematics, Vol. 1228* (Hackbusch, W. and Trottenberg, U., eds.), vol. 1228, pp. 166-201, Springer-Verlag, 1986.

<sup>16</sup>Drela, M., "Design and Optimization Method for Multi-Element Airfoils," Presented at AIAA/AHS/ASEE Aerospace Design Conference, Irvine, CA, AIAA Paper 93-0969. Feb. 16-19 1993.

<sup>17</sup>Hicks, R. M., "Transonic Wing Design Using Potential-Flow Codes - Successes and Failures," Presented at Presented at Business Aircraft Meeting & Exposition, Wichita, KS. AIAA Paper 95-0123, April. 7-10 1981.

<sup>18</sup>Kennelly, Jr., R. A., "Improved Method for Transonic Airfoil Design-by-Optimization," Presented at AIAA Applied Aerodynamics Conference, Danvers, MA, AIAA Paper 83-1864, July 13-15 1983.

<sup>19</sup>Gill, P. E., Murray, W., and Pitfield, R. A., "The Implementation of Two Revised Quasi-Newton Algorithms for Unconstrained Optimization," NAC 11, National Physical Laboratory, Division of Numerical Analysis and Computing, 1972.